ELSEVIER

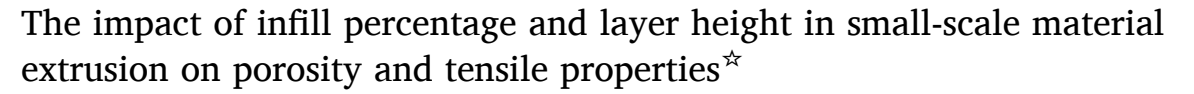
Contents lists available at ScienceDirect

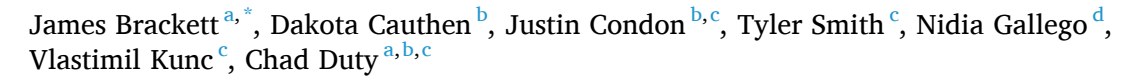
Additive Manufacturing

journal homepage: www.elsevier.com/locate/addma



Research Paper





- ^a The Bredesen Center for Interdisciplinary Research and Graduate Education, University of Tennessee, Knoxville, TN, United States
- ^b Mechanical, Aerospace, and Biomedical Engineering, University of Tennessee, Knoxville, TN, United States
- ^c Manufacturing Science Division, Oak Ridge National Laboratory, Oak Ridge, TN, United States
- ^d Chemical Sciences Division, Oak Ridge National Laboratory, Oak Ridge, TN, United States

ARTICLE INFO

Keywords:
3D Printing
Extrusion
Porosity
Mechanical Properties
Fused Filament Fabrication

ABSTRACT

Material extrusion additive manufacturing is prone to introducing porosity within the structure due to the layer-by-layer construction using elliptical beads of material. This open porosity ultimately plays a role in determining the mechanical properties of printed parts. The shape, size, and amount of porosity within a printed part is influenced by a variety of factors, including nozzle diameter, infill percentage, layer height, raster orientation, and print speed. While several studies have investigated these and other parameters' effects on mechanical performance and porosity, better understanding the interconnected relationships is crucial in balancing the various input parameters to achieve maximum strength. This work initially examined the influence of key print parameters (infill percentage and layer height) on the internal porosity of a printed Acrylonitrile Butadiene Styrene (ABS) part. Then, the print parameters and internal porosity were statistically correlated to final mechanical properties. Porosity was further classified as either open or closed to differentiate between connected voids in the mesostructure from isolated voids within the material itself. Mechanical performance increased with an increasing density and infill percentage, displaying a 224 % increase in elastic modulus and a 150 % increase in ultimate tensile strength. The contribution of layer height was found to be conditional upon the infill percentage.

1. Introduction

One of the most common methods of additive manufacturing (AM) is material extrusion, particularly Fused Filament Fabrication (FFF), of thermoplastic polymers. Due to the ease of implementation and affordability of FFF, it has been a popular choice for modelling, prototyping, and customized small-batch production applications [1]. However, layer-based construction using roughly elliptical beads introduces inherent inter-bead porosity and limits the resolution of FFF (100–150 μm) compared to most small-scale AM processes (10–25 μm) [2]. The amount of internal porosity is a function of printing parameters and

material properties and significantly impacts mechanical performance [3,4]. Likewise, print parameters display an independent effect on mechanical performance, demonstrating the need to consider both porosity and print settings simultaneously [5–8].

Porosity within a structure is a common defect that hinders mechanical performance, so the tendency of layer-by-layer construction to introduce structural porosity is an important consideration for AM. Deposition of adjacent elliptical beads, or rasters, can result in voids between rasters at the top and bottom of the ellipses, but this feature can also be intentionally used to leave space between rasters, i.e. an air gap, to control density and mechanical performance. One study by Hossain

^{*} This manuscript has been authored in part by UT-Battelle, LLC under Contract No. DE-AC05–000R22725 with the U.S. Department of Energy. The United States Government retains and the publisher, by accepting the article for publication, acknowledges that the United States Government retains a non-exclusive, paid-up, irrevocable, world-wide license to publish or reproduce the published form of this manuscript, or allow others to do so, for United States Government purposes. The Department of Energy will provide public access to these results of federally sponsored research in accordance with the DOE Public Access Plan (http://energy.gov/downloads/doe-public-access-plan).

^{*} Correspondence to: Room 205, 1512 Middle Dr, Knoxville, TN 37916, United States. E-mail address: jbracke4@vols.utk.edu (J. Brackett).

et al. [9] found that the air gap between rasters had a substantial impact on the Ultimate Tensile Strength (UTS) of Polycarbonate (PC). A negative air gap value eliminated pores between rasters, leading to a nearly defect-free specimen and improved UTS. However, this required time-consuming manual examinations to determine optimal processing parameters, which are likely to change with layer height or raster angle. In addition, porosity measurements relied on cross-sectional images to estimate its presence throughout the structure rather than direct measurements. Rankouhi et al. [10] found a similar relationship between UTS and porosity when using optical microscopy to study the "air-gap to material" ratio of printed ABS. Altering print settings to reduce the observed pore space from 5.3 % to 0.3 % improved both the elastic modulus and UTS by increasing the amount of material in the mesostructure. This illustrated the direct effect of porosity on mechanical performance through the simple absence of material that could otherwise contribute. Rodriguez et al. [11] found negative air gaps improved bonding, reduced void density, and could be used to control the internal mesostructure of an FFF-printed ABS part, providing a means to adjust performance through controlled porosity. Tanikella et al. [12] approached the issue from a macro point of view by tracking variations in mechanical properties as a function of mass using seven different thermoplastics. Comparing the actual deposited mass to theoretical density of the printed parts showed that UTS improved as samples approached theoretical density for all materials [12], which suggests the elimination of porosity improved mechanical performance. Since infill percentage directly influences the amount of material present in a given cross section, it has a similar influence on porosity and mechanical properties of printed structures. Alvarez et al. [13] observed an increase in both UTS and elastic modulus with increasing infill percentage in ABS, supporting the previously mentioned relationship between a denser internal structure and mechanical properties. The same trend was noted in additional studies using ABS and polylactic acid (PLA) despite changes in other parameters[14,15], suggesting that both air gap and infill percentage settings can be used to influence internal porosity. Even though the influence of internal voids on mechanical performance has been noted before these studies, there is still a lack of an in-depth investigation of the relationship between the mesostructural porosity and tensile performance.

Numerous studies have shown both raster and part orientation have a significant influence on mechanical properties. Using ABS, Huang and Singamneni [16] compared a range of unidirectional raster orientations from 0° to 90° and demonstrated a consistent decrease in UTS with increasing raster angle, which is a common finding when printing with ABS and unidirectional rasters [10,17]. When utilizing an alternating raster angle pattern and a 5 wt% carbon fiber-filled ABS (CF-ABS), the $0^{\circ}/90^{\circ}$ frequently demonstrated superior tensile properties compared to other commonly used patterns, such as a 45°/45° [18]. Wu et al. [19] found similar behavior printing with Poly-ether-ether-ketone (PEEK) for both tensile and bending testing, attributing a lower performance in the $30^{\circ}/-60^{\circ}$ and $45^{\circ}/-45^{\circ}$ patterns to additional shear stresses introduced by rasters neither parallel nor perpendicular to the load direction. In addition to reporting similar trends for raster angle patterns, Hossain et al. [9] also studied the effect of build orientation. The study consistently showed that a build orientation placing rasters in the loading direction and parallel to the printing surface while minimizing contact with the surface (the "XZY" orientation) provided the best tensile performance for printed PC parts. The cause was not immediately clear but was attributed to the greater presence of contours or perimeters used in this build orientation. While the orientation of printed parts and internal rasters is a critical factor, the impact is well understood.

The final shape of a bead after deposition also plays a critical role in mechanical performance through raster bonding, which is influenced by system parameters like layer height. In the same study by Ning et al. [18] using 5 wt% CF-ABS, a shorter layer height led to increased UTS values due to tighter packing and greater raster bonding. Similarly, the smaller of two layer heights also demonstrated a higher UTS in ABS-printed

parts [10]. However, Wu et al. [19] found that an intermediate layer height provided the optimal performance for PEEK-printed parts. In three similar studies, a layer height of 0.2 mm provided optimal properties for PC [20], the largest layer height (0.25 mm) resulted in the best mechanical response when printing polyamide 12 (PA12) [21], and the intermediate layer height (0.2 mm) provided optimal results for printed thermoplastic polyurethane (TPU) [22]. In contrast, a different study found that the minimal layer height (0.2 mm) created the best mechanical response in an ABS filled with hydrous magnesium silicate [23]. Although these findings could appear contradictory, it more likely indicates a dependence on material properties and additional print parameters. Regardless, it appears that the chosen layer height can directly impact the mechanical properties of an FFF-printed part.

While layer height, infill percentage, and internal porosity have each been studied, a clear interconnected relationship among print parameters, internal porosity, and mechanical performance has not been documented. Although parameters such as extrusion temperature [18, 24,25], material composition [19,24,26], air gap [9,10], and orientation [16,17] were also shown to affect porosity, they were held constant for this study. Furthermore, the influence of each parameter on mechanical performance should be considered independently to clarify the degree of influence each one had. This study investigates the influence of layer height and infill percentage on porosity and analyzes tensile performance as a function of layer height, infill percentage, and measured porosity.

2. Materials and methods

Although filaments used in FFF can be produced from a variety of thermoplastics, ABS is a common material because the material properties are comparable to many engineering plastics at a lower pricepoint [27]. FFF printing of ABS has been widely studied to understand the anisotropic properties, develop derivative ABS compounds for specific purposes, and determine the influence of various fillers [2,10–13, 16–19,25,26]. The material selected for this study was the Purple MH Build Series ABS Filament from Matter Hacker [28]. It was dried at 80 °C for at least four hours immediately prior to printing.

2.1. Printing conditions

All specimens were printed using a MakerGear M2 FFF system equipped with a 0.35 mm diameter nozzle. The ABS filament diameter was 1.75 mm. All prints used a $\pm 45^{\circ}$ infill orientation, an extrusion multiplier of 1.0, 0 perimeters, a 20 mm/s travel speed for solid infill, and 60 mm/s otherwise. Thermal conditions were also kept constant with bed and nozzle temperatures of 80 °C and 235 °C, respectively.

Since the ratio of the nozzle diameter to layer height is key in defining the scale of the structure, layer height and infill percentage were chosen as the variables for this study. In previous studies [13–18, 21–23] this ratio ranged from 1 to 6, so an intermediate range of 1.5–2.25 was investigated in the current study. Given a constant nozzle diameter of 0.35 mm, the resulting layer heights were calculated as shown in Table 1 below. Each layer height was printed at four infill percentages (85 %, 90 %, 95 %, and 100 %) which are commonly used in FFF [29], leading to a complete set of 16 different parameter combinations.

Table 1
Layer height selection.

Nozzle diameter (mm)	0.35			
Layer Height Ratio	1.5	1.75	2	2.25
Layer Heights (mm)	0.233	0.200	0.175	0.155

2.2. Print structure and specimen extraction

A flat, rectangular plate 111 mm by 89 mm (4.4 in by 3.5 in) was printed using each parameter set described above. Using a waterjet system and compatible.dxf file, eight tensile samples were extracted from each plate such that they retained the $\pm45^{\circ}$ raster orientation and met the Type V specifications found in ASTM D638-14 [30]. Cutting individual samples from a printed plate minimizes stress concentrations in the curved portions of traditional tensile geometries that reportedly leads to fractures in the transition zones when directly printing tensile samples [26]. While the top and bottom faces retained the "as-printed" surface roughness, the sides of the tensile specimens exposed to the waterjet cutting process had a different value. The "as-printed" surface (top) lying on the x-y plane had a measured roughness of 30.8 µm for a 100 % infill and 92.6 µm for an 85 % infill. The machined surfaces had an average measured roughness of 54.5 µm for the 100 % infill and 67.6 µm for the 85 % infill. Any specimens with visible imperfections were not included in mechanical analysis, resulting in approximately one in four samples being discarded due to printing imperfections, machining damage, or fracturing outside of the gage length. Three experimental sets experienced repeated delamination failures during printing: 0.155 mm layer height with 95 % and 100 % infills and 0.175 mm layer height with a 100 %. They were not included in the data analysis. In Fig. 1, the specimen extraction process is shown from printed plate to machining file to final remaining material. After machining, the tabs at the ends of each tensile bar were removed to ensure mass measurements included only the Type V geometry, as shown in Fig. 2. The thickness of all specimens was less than 4 mm, as required for a Type V geometry.

2.3. Density and porosity measurements

While porosity is defined as the empty space or voids within a structure, density can be defined in several ways. Two of the most commonly used versions are apparent density (ρ_{app}) and true density (ρ_{true}), which are differentiated by their method of volume calculations. As shown in Eqs. (1) and (2), ρ_{app} includes the volume of any open porosity, V_p , in addition to the volume of the material, V_m , whereas ρ_{true} disregards open porosity and measures only V_m [31,32]. Each equation uses only the material mass, m_m , disregarding any contributions from moisture by drying the samples at 80 °C for at least 4 h.

$$\rho_{app} = \frac{m_m}{V_m + V_p} \tag{1}$$

$$\rho_{true} = \frac{m_m}{V_m} \tag{2}$$

However, it is worth noting that two types of porosity can be present in a structure: open and closed. Open porosity, or the empty space measured by V_p , is accessible from the surface and generally infiltrated by a medium such as helium during true density measurements. Closed porosity typically includes voids or bubbles within the material and is therefore considered to be part of V_m for volume calculations. Fig. 3 below provides an exaggerated representation of open and closed

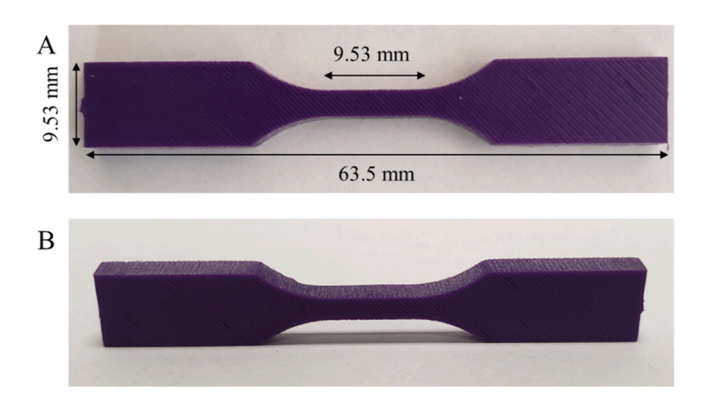


Fig. 2. A.) An extracted tensile specimen with labelled dimensions. B.) An alternate angle.

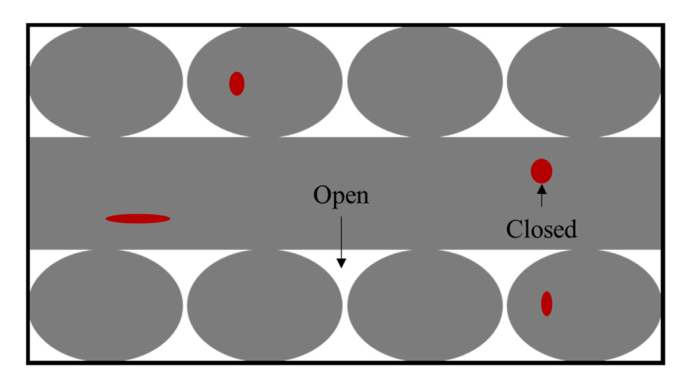


Fig. 3. A schematic illustrating the different types of porosity and density. The gray material represents a simple AM structure with alternating raster angles and incidental raster spacing.

porosity. In the case of apparent density measurements, the entire area within the black box would be included in volume calculations whereas true density would include only the volume of the gray material and enclosed red voids.

In this study, the true density was measured using a Quantachrome Instruments' Ultrapycnometer 1000, MUPY-15. Helium gas pycnometry provides accurate measurement of complex geometries by filling open porosity throughout the structure. Nine samples were measured: the starting filament and each layer height at both an 85 % and 100 % infill. The filament specimen was measured three times and compared to the average values of the 85 % infill and 100 % infill sets. These measurements acted as a theoretical maximum for apparent density, allowing the calculation of porosity. In addition, any difference between the true densities of the filament and the printed samples would indicate a change in closed porosity induced by the printing process.

The apparent density of each dogbone was found using dimensional measurements to calculate volume. This approach includes the open porosity within the final structure, as shown in Fig. 3 above, using Eq. (3) below.

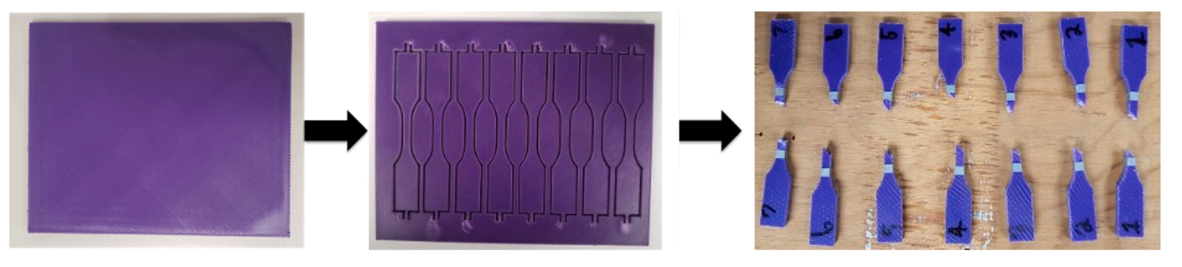


Fig. 1. The printed plate, waterjet results, and tested tensile specimens.

$$\rho_{app} = \frac{m_m}{V_m + V_p} = \frac{m_m}{V_{print}} = \frac{m_m}{t * A_{xy}}$$
(3)

Here, V_{print} incorporates both V_m and V_p and is obtained by multiplying the sample thickness, t, by the xy cross-sectional area, A_{xy} . The thickness, t, of each specimen was an average of five measurements made with calipers across the length of the tensile specimen. A_{xy} was a constant 471.2 mm^2 determined directly from the CAD file used to waterjet cut samples. Simple prismatic regions were found to compare favorably to machine file values, so A_{xy} was multiplied by t to determine volume. This approach was considered more accurate and practical than using calipers to physically measure complex curvatures. The mass of each dogbone was recorded to a 1 mg accuracy. The maximum ρ_{true} of the three sample sets was used as a theoretical limit to calculate the porosity present in each tensile sample. Eq. (4) shows the simple percent calculation.

Percent Porosity =
$$100 - \left(\frac{\rho_{app}}{\rho_{true}} \times 100\right)$$
 (4)

2.4. Tensile testing

Type V dogbones were mechanically tested on an MTS Criterion Series, Model 45 instrument using a 10 kN load cell and a testing rate of 1 mm/minute to achieve a nominal strain rate of 0.1 mm/(mm*min). Extension of the gauge length was tracked using an MTS LX 500 Laser Extensometer. No samples exhibited secondary peaks in strength, so the UTS was identified as the maximum recorded stress. Each reported value represented at least five acceptable tests.

3. Results and discussion

3.1. Density measurements

True density measurements using helium pycnometry indicated a measurable difference in the data sets, as shown in Table 2 below. The average true density of $100\,\%$ infill samples was greater than the average true density measured for filament and $85\,\%$ infill samples. An increase in density from filament to $100\,\%$ infill printed parts is likely the result of closed porosity within the filament being forced out of the structure by the dramatic reduction in cross-sectional area that occurs when extruding a $1.75\,\mathrm{mm}$ filament through a $0.4\,\mathrm{mm}$ nozzle. On the other hand, the reduced density seen in the $85\,\%$ infill samples is likely due to small, interstitial pores trapped by the geometry that were included in the measurements as closed porosity. While true density did not vary more than $2\,\%$ from the original filament, the $100\,\%$ infill value was treated as the theoretical maximum density and used as the baseline for all porosity calculations.

Fig. 4 shows the apparent density of the printed samples as a function of infill percentage for different layer heights. A two-part legend was utilized to distinguish both layer height and infill percentage in a single chart. Marker color identified the infill percentage used while the shape of the marker indicated the layer height. In every case, the apparent density was significantly lower than the theoretical maximum density, but the apparent density did increase as the infill percentage increased. Using a 100 % infill, the average porosity was measured to be 9 % whereas a maximum porosity of 21 % was observed in the 85 % infill. Conversely, layer height did not have a significant effect.

Fig. 5 shows the apparent density measurements at different layer

Table 2True density of original filament and printed samples.

Sample set	Filament	85 % Infill	100 % Infill
Average ρ _{true} (g/cc)	1.021	1.006	1.042
Standard Deviation (g/cc)	0.008	0.004	0.007

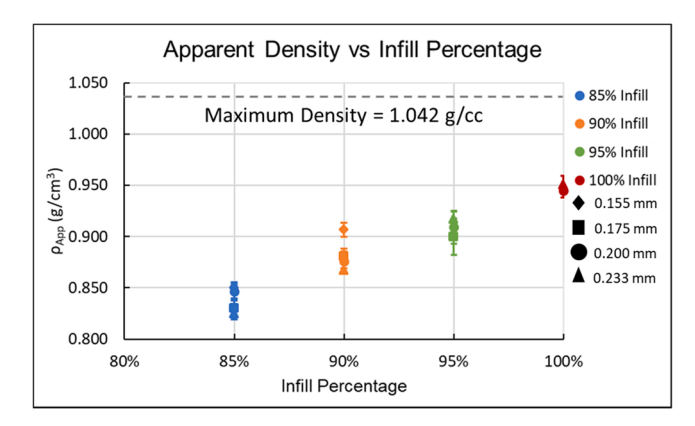


Fig. 4. Apparent density as a function of infill percentage. The dotted line represents the maximum measured true density observed in the 100~% infill samples.

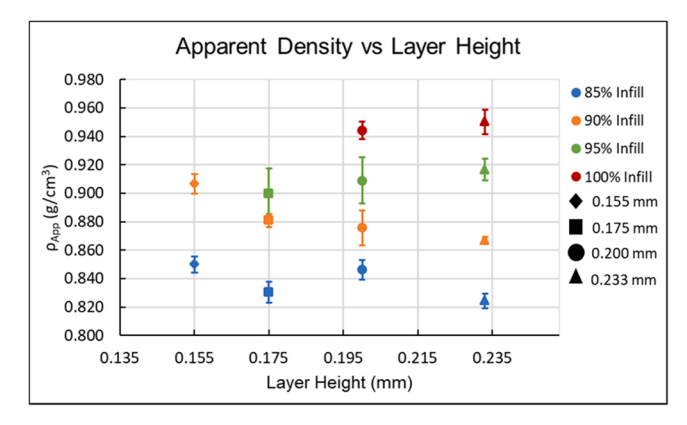


Fig. 5. Apparent density of the printed samples as a function of layer height.

heights to better illustrate the effect on open porosity. As before, there does not appear to be an overall relationship between layer height and measured open porosity. For instance, infill percentages of 95 % and 100 % had apparent densities that showed minimal variation when changing layer height. However, the 85 % and 90 % infill percentage samples each showed a consistent decrease in density with increasing layer height, resulting in a total decrease of 3 % and 5 % for the 85 % and 90 % infills, respectively. This contradictory behavior could be due to a critical point in infill percentage, after which any detrimental effects of larger rasters disappear. It could also be due to an increase in back pressure at higher infill percentages causing internal voids to be filled.

3.2. Parameter influence on young's modulus

As shown in Fig. 6, increasing the infill percentage can more than triple the Young's modulus. This trend had an ANOVA confidence level of 99 % (p = 0.0013), showing strong support for the correlation between infill percentage and Young's Modulus. The maximum of 1.66 GPa (95 % infill, 0.233 mm layer height) showed a 224 % increase compared to the minimum observed 0.51 GPa (85 % infill, 0.233 mm layer height). Although performance did not improve when increasing infill from 95 % to 100 %, the modulus values at 100 % remained within the standard deviation at 95 %. The resulting plateau had a tighter grouping of modulus measurements but otherwise indicates no advantage in increase infill percentage from 95 % to 100 %.

Fig. 7 shows layer height had two distinct impacts on the Young's modulus, depending upon infill percentage. The 85 % and 90 % infill samples exhibited a decrease in elastic modulus as layer height increased. When comparing a 0.155 mm layer height to a 0.233 mm

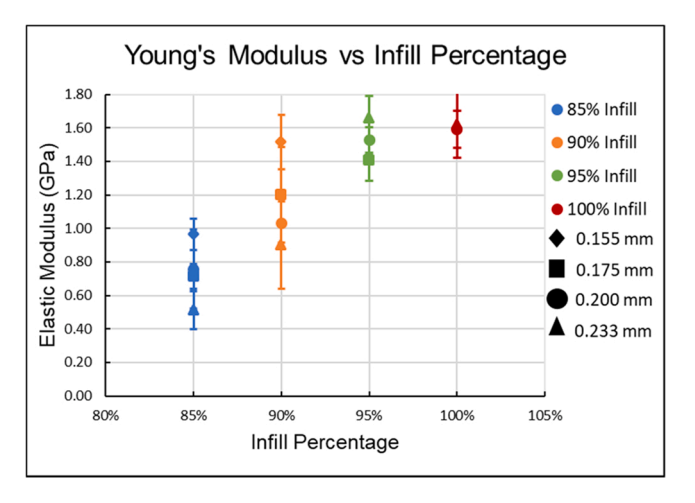
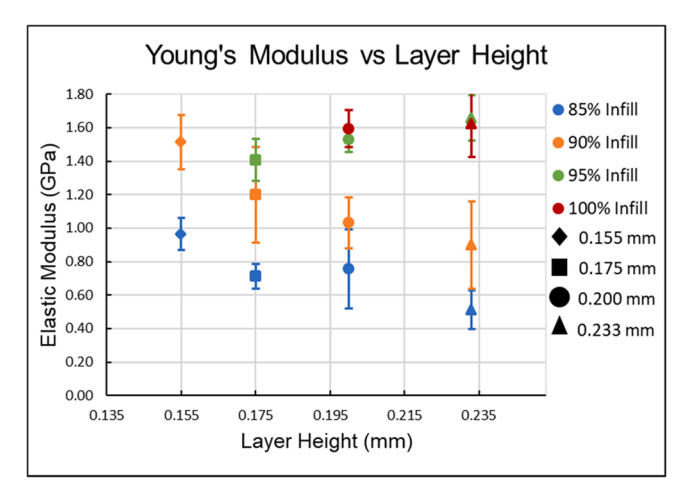


Fig. 6. The average Young's Modulus for each print as a function of infill percentage.



 $\begin{tabular}{ll} \textbf{Fig. 7.} & \textbf{The average Young's Modulus for each print as a function of layer height.} \end{tabular}$

height, Young's modulus decreased by 47 % (85 % infill) and 40 % (90 % infill). Following a typical Analysis of Variance (ANOVA) approach [33], there was a statistically significant (p = 0.03) relationship between layer height and elastic modulus for these two data sets. Conversely, the 95 % and 100 % infill data sets showed a slight increase in modulus with increasing layer height. A maximum of 1.68 GPa (95 % infill, 0.233 mm layer height) and minimum of 1.41 GPa (95 % infill, 0.175 mm layer height) demonstrated an increase of 15 %. However, the increase in modulus was not statistically significant due to large variation. As mentioned previously, this likely indicates the existence of a threshold between 90 % and 95 % infill levels after which the contributions of an increasing layer height to elastic modulus become irrelevant or beneficial rather than detrimental. Thus, decreasing layer height contributed to increased elastic moduli when below this threshold. The likelihood of a threshold is further reinforced by comparing these results to similar studies. For specimens printed with a 100 % infill, the nozzle diameter to layer height ratio was consistently < 2 in the samples with an optimized mechanical response [20-22] while those printed at lower infill percentage favored ratios > 2 [23]. Therefore, these results provide supported evidence of a threshold infill percentage between 90 % and 95 % at which the contributions of layer height change.

3.3. Parameter influence on UTS

Measured UTS values exhibited similar trends to those seen for

Young's Modulus. In Fig. 8, UTS increased by roughly 150 % (12-29 MPa) as infill percentage increased from 85 % to 100 %. As such, infill percentage displayed a direct influence (p = 0.00001) on UTS, showing an almost linear relationship. Additionally, average UTS showed less variability as infill percentage increased, which was not present in the modulus data. Plotting UTS as a function of layer height in Fig. 9 revealed two distinct and familiar trends. With the 85 % and 90 % infill data sets, UTS decreased with increasing layer height, displaying a statistically significant (p = 0.003) correlation between smaller layer heights and increased UTS. The average UTS decreased by 31 % (85 %infill) and 34 % (90 % infill) when comparing the 0.155 mm layer height average to 0.233 mm layer height average. However, the 95 % and 100 $\,$ % infill sets showed no change in UTS with differing layer heights. Considering the connections discussed in Section 3.2, the nozzle diameter to layer height ratio appears to have a much less pronounced effect on UTS at the highest infill percentages while exhibiting the same increase in performance at ratios > 2. This suggests that sufficiently low infill percentages could use layer height to tailor mechanical properties.

3.4. Consideration of density with respect to moduli and UTS

In some instances, considering mechanical performance alone is insufficient for assessing functional performance. Considering elastic modulus and UTS as a function of the component's density ensures the inclusion of mass in design considerations. This consideration of specific properties (material properties treated as a function of density) is crucial for industries that seek to minimize mass, such as aerospace. For this study, both elastic modulus and UTS were plotted as a function of apparent density to illustrate trends in the calculated specific moduli and UTS of the printed samples. A two-part legend was utilized to distinguish both layer height and infill percentage in one chart. Marker color identified the infill percentage used while the shape of the marker indicated the layer height. As shown by Fig. 10, the modulus demonstrated a gradual increase with density but appeared to plateau after reaching infill levels greater than 95 %. The deviation present in the 95 % infill and 100 % infill samples indicated similar mechanical performance, suggesting that any further increase in density provided little mechanical benefit. As a result, there was approximately a 6 % reduction in the specific modulus when comparing the 95 % infill averages to the 100 % infill averages. The specific moduli demonstrated an increase of 192 % with a minimum (0.62 GPa/(g/cm³) at 85 % infill) and maximum (1.81 Gpa/(g/cm³) at 95 % infill) both having a layer height of 0.233 mm. As before, this indicted the possibility of sub-trends within the complete data set. Considering only the samples with an 85 % and 90 % infills, the specific moduli increased with decreasing layer height within each infill percentage, but a greater infill percentage did not

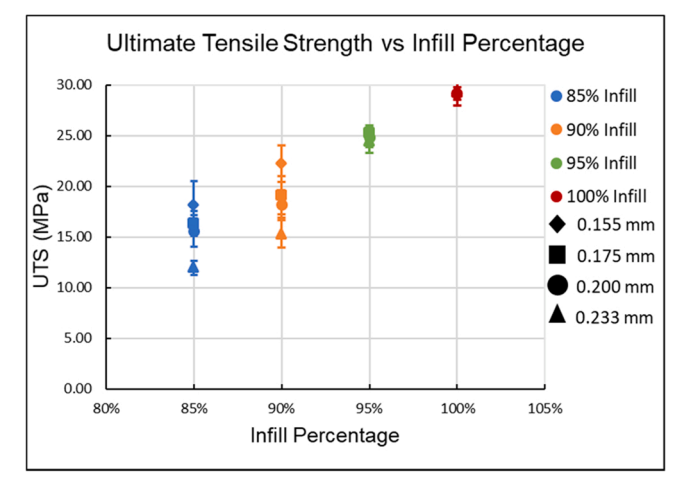


Fig. 8. The average UTS of each print as a function of infill percentage.

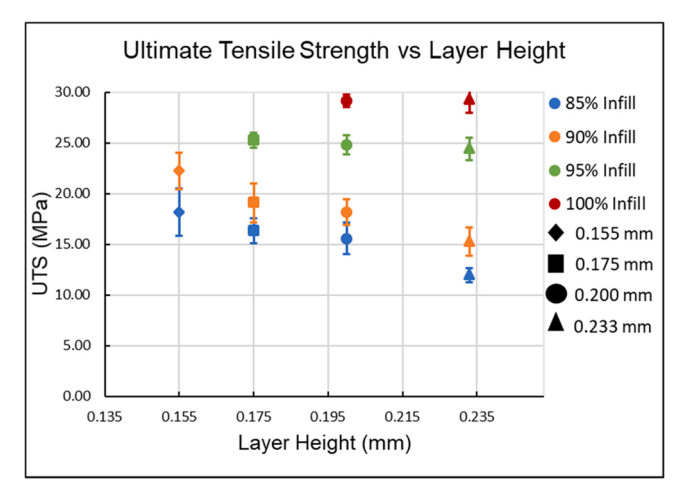


Fig. 9. The UTS of each print as a function of layer height.

necessarily lead to a higher modulus. For example, an 85 % infill at a 0.155 mm layer height outperformed a 90 % infill at 0.233 mm layer height by 8 %. Even though the 90 %, 0.233 mm sample exhibited less porosity, the smaller layer height led to an improved performance that compensated for the additional porosity. However, once the 95 % infill was reached, the trend reversed. The increasing density provided by larger layer heights correlated with improved moduli and, therefore, an improved specific modulus. This phenomenon correlates well with the previously observed trends in effect of nozzle diameter to layer height ratio on final mechanical properties. This suggests that, in addition to the general influence of porosity on mechanical performance, layer

height and infill percentage affected porosity and performance independently.

Similar patterns were present for UTS in Fig. 11, which showed a clear increase in UTS with increasing density. With only a 15 % increase in apparent density, the UTS increased by 144 % from 11.9 MPa (85 % infill with 0.233 mm layer height) to 29.3 MPa (100 % infill with 0.233 mm layer height). Additionally, the 95 % and 100 % infills each had standard deviation within the sample sets that suggests a similar mechanical performance despite changes in layer height. For specimens with 85 % and 90 % infills however, there was a significant difference in performance that was connected to layer height. A shorter layer height reduced porosity within the samples and led to increased specific UTS values, but once again the taller layer heights in the 90 % infill group underperformed the shorter layer heights with an 85 % infill. This occurred despite the reduced porosity in the 90 % infill samples, indicating the strength gains did not keep pace with the rate of mass added. Specific UTS continued to improve with increasing infill percentage, but the 95 % infill and 100 % infill did not exhibit any internal trends related to layer height. Again, this matches the trends for nozzle diameter to layer height ratio seen previously.

4. Conclusions

This study provided one of the first in-depth analysis of the connections between print parameters, porosity, and tensile properties. The print parameters of interest were infill percentage and layer height, producing a porosity that ranged from 9 % to 22 %. Infill percentage had the largest impact on apparent density while changes in layer height led to relatively small differences in porosity between samples of the same infill percentage. Although this study focused on tensile properties, the

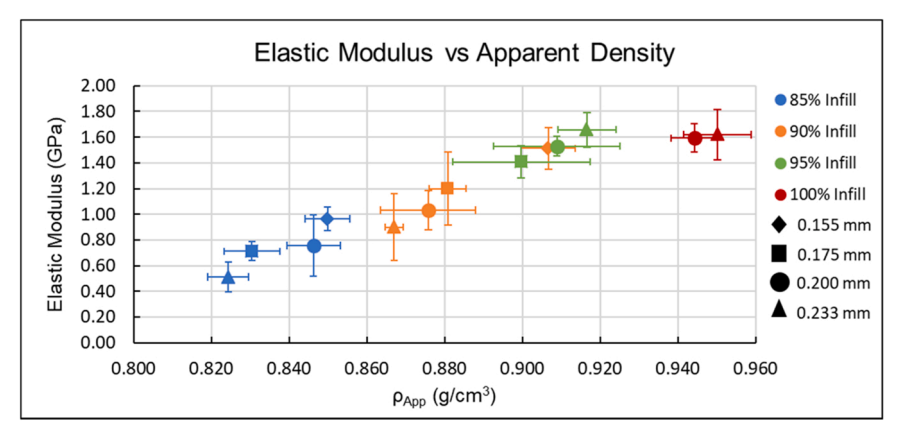


Fig. 10. The specific moduli of tested tensile samples.

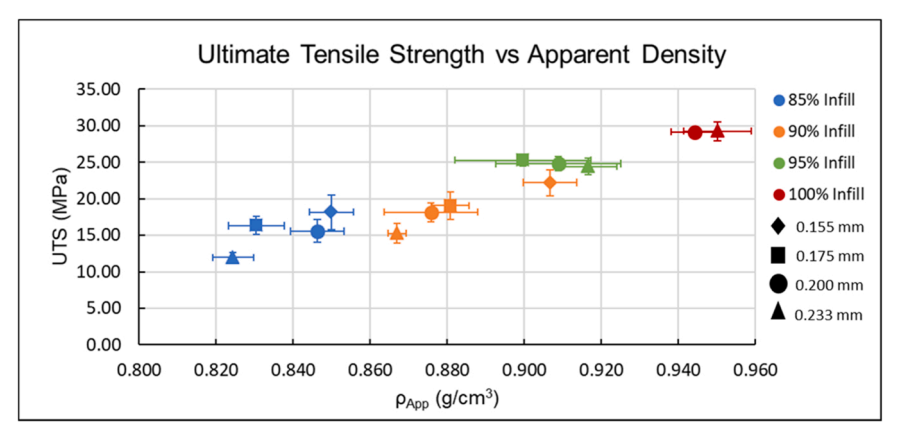


Fig. 11. The specific UTS of tested tensile samples.

porosity may also have an impact on other characteristics important for specific applications, such as CTE, ductility, vacuum integrity, etc., as will be evaluated in future work. The elastic modulus increased by over a factor of three and UTS increased by more than 2x, primarily due to increased infill percentage. An increased infill percentage consistently reduced porosity and had strong statistical correlation to higher UTS and elastic modulus. For 85 % and 90 % infill percentages, layer height had a statistically significant influence on UTS and elastic modulus, demonstrating increased performance at smaller layer heights. This was attributed to an observed reduction in porosity and the nozzle diameter to layer height ratio. The maximum specific moduli and specific UTS were observed at a 95 % infill percentage because the increased mass at 100 % infill percentage produced a minimal increase in mechanical properties. This interplay between porosity and mechanical properties is important for applications that are focused on optimizing the strengthto-weight ratio.

In addition, assessing mechanical performance as a function of density demonstrated the benefit of including porosity in mechanical characterization. Since measured apparent densities were significantly lower than the true density of the material, using a reported material density in various studies may be misleading, suggesting that AM parts may be better represented by calculated apparent densities. As such, mechanical characterization could benefit from considering porosity and apparent density as an integral part of the process.

CRediT authorship contribution statement

Vlastimil Kunc: Supervision, Resources, Funding acquisition, Conceptualization. Chad Duty: Writing – review & editing, Visualization, Supervision, Resources, Methodology, Funding acquisition, Conceptualization. Dakota Cauthen: Visualization, Validation, Methodology, Investigation, Formal analysis, Data curation. Justin Condon: Validation, Software, Resources. Tyler Smith: Supervision, Software, Resources. Nidia Gallego: Validation, Supervision, Resources, Methodology, Data curation. James Brackett: Writing – review & editing, Writing – original draft, Validation, Supervision, Project administration, Methodology, Investigation, Formal analysis, Data curation, Conceptualization.

Declaration of Competing Interest

The authors declare the following financial interests/personal relationships which may be considered as potential competing interests: James Brackett reports financial support was provided by US Department of Energy. A co-author, Dr. Chad Duty, is a currently serving as an editor for Additive Manufacturing. - James Brackett.

Data Availability

Data will be made available on request.

Acknowledgements

Research sponsored by the U.S. Department of Energy, Office of Energy Efficiency and Renewable Energy, Industrial Technologies Program, under contract DE-AC05-00OR22725 with UT-Battelle, LLC. This material was also based upon work supported by the National Science Foundation under Grant No. 2055529 and supported in part by Oak Ridge Institute for Science and Education through the Higher Education Research Experiences Program (HERE). Further thanks to the University of Tennessee – Knoxville Innovation & Collaboration Studio for their assistance.

References

- B. Wendel, D. Rietzel, F. Kuhnlein, R. Feulner, G. Hulder, E. Schmachtenberg, Additive processing of polymers, Macromol. Mater. Eng. 293 (2008) 799–809, https://doi.org/10.1002/mame.200800121.
- [2] S.C. Ligon, R. Liska, J. Stampfl, M. Gurr, R. Mulhaupt, Polymers for 3d printing and customized additive manufacturing, Chem. Rev. 117 (15) (2017) 10212–10290, https://doi.org/10.1021/acs.chemrev.7b00074.
- [3] J.A. Choren, S.M. Heinrich, M.B. Silver-Thorn, Young's modulus and volume porosity relationships for additive manufacturing applications, J. Mater. Sci. 48 (15) (2013) 5103–5112, https://doi.org/10.1007/s10853-013-7237-5.
- [4] A. Balagopal, R.K. Mandal, P.K. Singh, P. Jain, Effects of porosity on mechanical property and specific strength of monolithic carbon fibre reinforced polylactic acid and acrylonitiril butadiene styrene components fabricated using additive manufacturing technique, Int. J. Sci. Res. Mech. Mater. Eng. 4 (5) (2020) 29–40. (http://iisrmme.com/JJSRMME20457).
- [5] J. Kechagias, D. Chaidas, N. Vidakis, K. Salonitis, N.M. Vaxevanidis, Key parameters controlling surface quality and dimensional accuracy: a critical review of fff process, Mater. Manuf. Process. 37 (9) (2022) 963–984, https://doi.org/ 10.1080/10426914.2022.2032144.
- [6] J.D. Kechagias, S.P. Zaoutsos, D. Chaidas, N. Vidakis, Multi-parameter optimization of pla/coconut wood compound for fused filament fabrication using robust design, Int. J. Adv. Manuf. Technol. 119 (7–8) (2022) 4317–4328, https:// doi.org/10.1007/s00170-022-08679-2.
- [7] S.B. Balani, F. Chabert, V. Nassiet, A. Cantarel, Influence of printing parameters on the stability of deposited beads in fused filament fabrication of poly(lactic) acid, Addit. Manuf. 25 (2019) 112–121, https://doi.org/10.1016/j.addma.2018.10.012.
- [8] A.M. Peterson, Review of acrylonitrile butadiene styrene in fused filament fabrication: a plastics engineering-focused perspective, Addit. Manuf. 27 (2019) 363–371, https://doi.org/10.1016/j.addma.2019.03.030.
- [9] M.S. Hossain, D. Espalin, J. Ramos, M. Perez, R. Wicker, Improved mechanical properties of fused deposition modeling-manufactured parts through build parameter modifications, J. Manuf. Sci. Eng. - Trans. ASME 136 (6) (2014), https://doi.org/10.1115/1.4028538.
- [10] B. Rankouhi, S. Javadpour, F. Delfanian, T. Letcher, Failure analysis and mechanical characterization of 3d printed abs with respect to layer thickness and orientation, J. Fail. Anal. Prev. 16 (3) (2016) 467–481, https://doi.org/10.1007/ s11668-016-0113-2.
- [11] J.F. Rodriguez, J.P. Thomas, J.E. Renaud, Characterization of the mesostructure of fused-deposition acrylonitrile-butadiene-styrene materials, Rapid Prototyp. J. 6 (3) (2000) 175–185. https://doi.org/10.1108/13552540010337056.
- [12] N.G. Tanikella, B. Wittbrodt, J.M. Pearce, Tensile strength of commercial polymer materials for fused filament fabrication 3d printing, Addit. Manuf. 15 (2017) 40–47, https://doi.org/10.1016/j.addma.2017.03.005.
- [13] K. Alvarez, R. Lagos, M. Aizpun, Investigating the influence of infill percentage on the mechanical properties of fused deposition modelled abs parts, Ing. Investig. 36 (2016) 110–116, https://doi.org/10.15446/ing.investig.v36n3.56610.
- [14] A. Rodríguez-Panes, J. Claver, A.M. Camacho, The influence of manufacturing parameters on the mechanical behaviour of pla and abs pieces manufactured by fdm: a comparative analysis, Materials 11 (8) (2018) 1333, https://doi.org/ 10.3390/ma11081333.
- [15] M. Samykano, S.K. Selvamani, K. Kadirgama, W.K. Ngui, G. Kanagaraj, K. Sudhakar, Mechanical property of fdm printed abs: Influence of printing parameters, Int. J. Adv. Manuf. Technol. 102 (9–12) (2019) 2779–2796, https://doi.org/10.1007/s00170-019-03313-0.
- [16] B. Huang, S. Singamneni, Raster angle mechanics in fused deposition modelling, J. Compos. Mater. 49 (3) (2015) 363–383, https://doi.org/10.1177/ 0021998313519153.
- [17] T. Letcher, B. Rankouhi, S. Javadpour, Experimental study of mechanical properties of additively manufactured abs plastic as a function of layer parameters, 2015. (https://doi.org/10.1115/IMECE2015-52634).
- [18] F. Ning, W. Cong, Y. Hu, H. Wang, Additive manufacturing of carbon fiber-reinforced plastic composites using fused deposition modeling: effects of process parameters on tensile properties, J. Compos. Mater. 51 (4) (2017) 451–462, https://doi.org/10.1177/0021998316646169.
- [19] W. Wu, P. Geng, G. Li, D. Zhao, H. Zhang, J. Zhao, Influence of layer thickness and raster angle on the mechanical properties of 3d-printed peek and a comparative mechanical study between peek and abs, Materials 8 (9) (2015) 5834–5846, https://doi.org/10.3390/ma8095271.
- [20] N. Vidakis, M. Petousis, J.D. Kechagias, A comprehensive investigation of the 3d printing parameters' effects on the mechanical response of polycarbonate in fused filament fabrication, Prog. Addit. Manuf. (2022) 10, https://doi.org/10.1007/s40964-021-00258-3.
- [21] N. Vidakis, M. Petousis, J.D. Kechagias, Parameter effects and process modelling of polyamide 12 3d-printed parts strength and toughness, Mater. Manuf. Process. (2022) 1–12, https://doi.org/10.1080/10426914.2022.2030871.
- [22] J.D. Kechagias, N. Vidakis, M. Petousis, Parameter effects and process modeling of fff-tpu mechanical response, Mater. Manuf. Process. (2021), https://doi.org/ 10.1080/10426914.2021.2001523.
- [23] K.G.J. Christiyan, U. Chandrasekhar, K. Venkateswarlu, A study on the influence of process parameters on the mechanical properties of 3d printed abs composite, in: Proceedings of the 2nd International Manufacturing Engineering Conference (iMEC)/3rd Asia-Pacific Conference on Manufacturing Systems (APCOMS), Kuala Lumpur, MALAYSIA, 114, 2016. https://doi.org/10.1088/1757-899x/114/1/012109).

- [24] B. Wittbrodt, J.M. Pearce, The effects of pla color on material properties of 3d printed components, Addit. Manuf. 8 (2015) 110–116, https://doi.org/10.1016/ i.addma.2015.00.006
- [25] Q. Sun, G.M. Rizvi, C.T. Bellehumeur, P. Gu, Effect of processing conditions on the bonding quality of fdm polymer filaments, Rapid Prototyp. J. 14 (2) (2008) 72–80, https://doi.org/10.1108/13552540810862028.
- [26] S.H. Ahn, M. Montero, D. Odell, S. Roundy, P.K. Wright, Anisotropic material properties of fused deposition modeling abs, Rapid Prototyp. J. 8 (4) (2002) 248–257, https://doi.org/10.1108/13552540210441166.
- [27] E.-K. Karahaliou, P.A. Tarantili, Preparation of poly (acrylonitrile-butadiene-styrene)/montmorillonite nanocomposites and degradation studies during extrusion reprocessing, J. Appl. Polym. Sci. 113 (4) (2009) 2271–2281, https://doi.org/10.1002/app.30158.
- [28] MatterHackers, Purple mh build series abs filament 1.75mm (1kg), 2019. Available: https://www.matterhackers.com/store/3d-printer-filament/175mm-abs-filament-purple-1-kg.
- [29] N.A. Fountas, I. Papantoniou, J.D. Kechagias, D.E. Manolakos, N.M. Vaxevanidis, Modeling and optimization of flexural properties of fdm-processed pet-g specimens using rsm and gwo algorithm, Eng. Fail. Anal. 138 (2022), https://doi.org/ 10.1016/j.engfailanal.2022.106340.
- [30] ASTM D638-14, Standard test method for tensile properties of plastics, ASTM International, West Conshohocken, PA, 2014. (https://doi.org/10.1520/D0 638-14)
- [31] J. Rodríguez-Ramírez, L. Méndez-Lagunas, A. López-Ortiz, S.S. Torres, True density and apparent density during the drying process for vegetables and fruits: a review, J. Food Sci. 77 (12) (2012) R146–R154, https://doi.org/10.1111/j.1750-3841.2012.02990 x
- [32] ASTM D6436–14, Standard guide for reporting properties for plastics and thermoplastic elastomers, ASTM International, West Conshohocken, PA, 2019. (https://doi.org/10.1520/D6436-14).
- [33] I. Bross, Critical levels, statistical language and scientific inference (Foundations of statistical inference.). Toronto: Holt, Rinehart, & Winston of Canada, Ltd., 1971.